Research Square

Preprints are preliminary reports that have not undergone peer review.
They should not be considered conclusive, used to inform clinical practice,
or referenced by the media as validated information.

Metric-Dependent Dosimetric Divergence Between 106Ru and 125I Eye Plaques: A TOPAS Monte Carlo Dose-Volume Histogram Analysis

Shahab Atefi

Shahab.atefi01@universitadipavia.it

University of Pavia

Saleh Rouhi

Kermanshah University of Medical Sciences

Parvin Ahmadi

Shahed University

Research Article

Keywords: TOPAS, Monte Carlo simulation, Brachytherapy, Ophthalmic plaque, Dose-volume histogram, Uveal melanoma

Posted Date: November 23rd, 2026

DOI: https://doi.org/10.21203/rs.3.rs-11724309/v1

License: This work is licensed under a Creative Commons Attribution 4.0 International License.
Read Full License

Additional Declarations: No competing interests reported.

Metric-Dependent Dosimetric Divergence Between 106Ru and 125I Eye Plaques: A TOPAS Monte Carlo Dose-Volume Histogram Analysis

Abstract

Uveal melanoma is commonly treated with episcleral plaque brachytherapy, yet photon-emitting and beta-emitting plaques are rarely compared across the full clinically relevant range of tumor depth. This study compared dose-volume histogram (DVH) characteristics of an ^{125}I Collaborative Ocular Melanoma Study (COMS) plaque and an ^{106}Ru Concave Circular Applicator (CCA) plaque using TOPAS Monte Carlo simulations in an eye phantom. Seven tumor apical heights (4 to 12 mm) were simulated. Each plaque was independently normalized to 85 Gy at 4 mm depth on the central axis, a reference achievable by both sources. Tumor and organ-at-risk DVHs were extracted for the lens, cornea, and optic nerve. The ^{106}Ru plaque delivered a higher median tumor dose than ^{125}I through 7 mm (502.8 vs 202.7 Gy at 4 mm; 157.2 vs 97.2 Gy at 7 mm), but its apex dose was lower at every height beyond 4 mm (2.47 vs 35.84 Gy at 7 mm; 1.86 vs 29.25 Gy at 8 mm). The D_{50}/D_{98} heterogeneity ratio peaked at 52.6 at 7 mm for ^{106}Ru vs 2.5 for ^{125}I. Mean organ-at-risk doses were approximately tenfold lower with ^{106}Ru at all heights (lens 1.63 vs 15.8 Gy). The two plaques are indistinguishable by prescription-dose coverage, and a comparison based on that metric alone would incorrectly conclude that they are equivalent. Photon and beta plaques differ in the shape rather than the depth of their intratumoral dose distributions, and comparative plaque dosimetry should report sub-prescription coverage and near-minimum dose rather than prescription-dose coverage alone.

Keywords: TOPAS; Monte Carlo simulation; Brachytherapy; Ophthalmic plaque; Dose-volume histogram; Uveal melanoma

1. Introduction

Uveal melanoma is the most common primary intraocular malignancy in adults, and its management sits at the intersection of oncologic control and functional preservation [1]. Episcleral plaque brachytherapy has become a globally established, globe-conserving alternative that delivers highly localized irradiation to the tumor base while minimizing dose to uninvolved ocular structures [2]. The clinical rationale for plaque brachytherapy rests on its capacity to achieve tumor control rates comparable to enucleation while preserving the eye and, in many patients, useful vision.

The Collaborative Ocular Melanoma Study (COMS) remains the definitive randomized evidence in this field. In the medium-sized choroidal melanoma trial, 1,317 patients were randomized to enucleation or iodine-125 (^{125}I) brachytherapy, and no significant survival difference was observed through 12 years of follow-up [3]. At 12 years, melanoma-related mortality was 21% in the brachytherapy arm versus 17% in the enucleation arm—a difference that did not approach statistical significance and that threshold analyses have shown would require implausibly large mortality shifts to become significant [4]. Approximately 90% of brachytherapy-treated patients achieved local tumor control and 88% retained the globe at 5 years [3]. The COMS therefore established ^{125}I plaque brachytherapy at a prescription dose of 85 Gy to the tumor apex as the reference standard for medium-sized uveal melanoma [5].

The physical characteristics of the isotopes used in ophthalmic plaques are central to the therapeutic ratio. ^{125}I emits a low-energy photon spectrum (mean photon energy ~28 keV) that produces an extremely steep dose gradient: distal tissues are spared, but the lens, macula, fovea, and optic nerve lie within millimeters of a rapidly changing field. Radiation cataract, maculopathy, optic neuropathy, and retinopathy therefore remain the dose-limiting toxicities that constrain deliverable tumor dose. Beta-emitting isotopes specifically ruthenium-106 (^{106}Ru) offer a complementary dosimetric profile. Their short particle range concentrates dose within the tumor volume and limits penetration to sensitive distal structures, making them particularly attractive for superficial and small-to-medium tumors. Among beta-emitting ophthalmic plaques, the Concave Circular Brachytherapy (CCB) and Concave Circular Applicator (CCA) models (from BEBIG) are clinically used for uveal melanoma and has been shown in Monte Carlo studies to produce a uniform intratumoral dose distribution for tumor coverage and organ-at-risk (OAR) sparing depending on tumor height [6-8].

The coexistence of photon-emitting and beta-emitting plaque systems raises a practical dosimetric question: for a given tumor depth, which isotope–plaque combination provides the more favorable balance between target coverage and OAR exposure? Answering this question requires volumetric dose metrics rather than prescription-point doses alone. Dose-volume histograms (DVHs) provide exactly this information by quantifying the dose received by a specified percentage of a structure volume, and they have been incorporated into advanced ophthalmic plaque treatment-planning systems for both ^{125}I COMS and ^{106}Ru plaques. DVH-based comparisons are therefore well suited to capture the steep gradients and small structure volumes that characterize ocular brachytherapy.

Monte Carlo simulation is the appropriate computational framework for such comparisons. Despite the clinical availability of both plaque types, no study has directly compared their DVH-derived dosimetric parameters as a continuous function of tumor apical height using a single validated Monte Carlo engine. A validated simulation platform enables the consistent, geometry-specific dose scoring needed for a fair ^{125}I-versus-^{106}Ru DVH comparison.

Prior work has either examined each plaque type in isolation, compared plaque models within a single isotope, or evaluated bi-radionuclide designs without a depth-stratified DVH framework spanning the clinically relevant tumor-height range [9-11]. The present study used TOPAS Monte Carlo [12] simulations to compare DVH-derived target and OAR metrics between the ^{106}Ru CCA plaque and the ^{125}I COMS plaque across tumor apical heights of 4, 5, 6, 7, 8, 10, and 12 mm. The specific aim is to determine whether the dosimetric advantage of

one plaque type is preserved, attenuated, or reversed as tumor depth increases, thereby informing isotope and plaque selection for depth-stratified uveal melanoma treatment.

2. Methods

2.1. Simulation framework

All dose calculations were performed with TOPAS (TOol for PArticle Simulation) [12, 13], a Geant4-based Monte Carlo platform [14] developed specifically for medical physics applications. TOPAS provides a parameterized, non-programmatic interface for geometry construction, physics configuration, particle tracking, and event-by-event scoring, which enables reproducible and auditable simulation definitions. The present study used OpenTOPAS version 4.0 (https://github.com/OpenTOPAS), a community-maintained distribution derived from the TOPAS 3.9 development lineage. The platform has been extensively benchmarked for brachytherapy, including COMS-style ophthalmic plaques [15].

2.2. Physics List

Electromagnetic interactions were modeled with the *g4em-livermore* module, which implements the Geant4 *G4EmLivermorePhysics* class and the Livermore low-energy electromagnetic models [16]. This configuration is optimized for photon and electron transport down to approximately 250 eV and is therefore appropriate for the low-energy photon spectrum of ^{125}I (mean photon energy ~28 keV) and the beta spectrum of ^{106}Ru (endpoint energy 3.54 MeV). For photons, photoelectric absorption, Compton scattering, Rayleigh scattering, and pair production were enabled. For electrons and positrons, ionization, bremsstrahlung, multiple Coulomb scattering, and excitation were enabled.

Atomic de-excitation was handled by the g4decay module (Geant4 *G4DecayPhysics* class), which simulates fluorescence X-ray emission and Auger electron release following inner-shell vacancy production. This is a non-negligible contribution for ^{125}I, whose dosimetry is sensitive to the low-energy photon and electron cascade emitted after photoelectric absorption in the gold-alloy plaque backing and in tissue.

A production range cut of 0.1 mm was applied to secondary particles. Particles whose projected range falls below this threshold are not tracked further; their residual kinetic energy is deposited locally at the termination point. This cut value represents a deliberate compromise between computational efficiency and spatial fidelity in the millimeter-scale structures of the eye, and it is consistent with values reported for ocular brachytherapy simulations [11].

2.3. Plaque Models

Two clinically deployed ophthalmic plaque systems were modeled: the beta-emitting ^{106}Ru CCA plaque and the photon-emitting ^{125}I COMS plaque. Both were positioned at the same location on the scleral surface overlying the tumor base, with the plaque concavity conforming to the globe and the plaque central axis aligned with the tumor apex.

2.3.1 ^{106}Ru CCA plaque

The CCA plaque was modeled to BEBIG clinical specifications [17]. The CCA was selected because it is the most widely used beta-emitting ophthalmic plaque in clinical practice and because its concave geometry provides conformal coverage of the tumor base while limiting dose to the lens, cornea, and optic nerve. The modeled plaque comprises a 0.1 mm silver window, a 0.2 mm ^{106}Ru-coated silver foil, and a 0.7 mm silver backing. Its total diameter is 15.3 mm, of which 14.9 mm constitutes the active diameter. The activity is uniformly distributed across the foil [7, 17].

^{106}Ru (T½ = 373.6 d) decays by beta emission to ^{106}Rh (T½ = 30.1 s), which in turn decays to stable ^{106}Pd [18]. Because the parent half-life greatly exceeds that of the daughter, the two nuclides reach transient equilibrium within the plaque, and the ^{106}Rh beta spectrum dominates the dose delivered to the tumor. The ^{106}Rh beta endpoint of 3.54 MeV was therefore used to define the emission spectrum in the simulation, with the minor ^{106}Ru branch also included (^{106}Ru endpoint = 0.0394 MeV). ^{106}Rh also emits a low-abundance photon component (principally ~0.512 and ~0.622 MeV gammas) that was transported in the simulation but contributes negligibly to local tumor dose.

2.3.2 ^{125}I COMS plaque

The ^{125}I plaque was modeled as a 14 mm-diameter (7 mm-radius) gold-alloy COMS cup (Modulay: Au 77%, Ag 14%, Cu 8%, Pd 1% by mass; ρ = 15.8 g/cm³) loaded with 13 cylindrical ^{125}I seeds in the standard COMS loading pattern [5]. Each seed was modeled on the Imagyn IS-12501 geometry specified in the AAPM TG-43U1 report [19]: a 4.5 mm-long titanium capsule (0.05 mm wall, 0.4 mm end caps, outer radius 0.4 mm) enclosing five silver microspheres (radius 0.3 mm) with ^{125}I uniformly adsorbed on their surfaces. The 0.05 mm titanium encapsulation is sufficient to stop all emitted conversion and Auger electrons, so the seeds were treated as pure photon sources. The active length of the IS-12501 is 3.4 mm. The ^{125}I photon spectrum was taken from TG-43U1 [19] and comprises the following emissions (energy; relative intensity per 100 decays): 27.20 keV (40.6), 27.47 keV (75.7), 30.98 keV (20.2), 31.71 keV (4.39), and 35.49 keV (6.68).

2.4. Computational Eye Phantom

Following Ref. [6], the globe was modeled as a 12 mm-radius sphere of ICRP soft tissue with concentric anatomical layers (thickness and density in parentheses): sclera (1.0 mm; ρ = 1.12 g/cm³), choroid (0.3 mm; ρ = 1.07 g/cm^3), retina (10.7–10.5 mm; ρ = 1.07 g/cm³), and a vitreous body (water) filling the interior. A biconvex crystalline lens (ρ = 1.07 g/cm³; semi-axes 4.0 × 1.8 × 4.9 mm) was positioned near the cornea, iris, and a toroidal ciliary body. The macula was modeled as a thin retinal disk at the posterior pole, and the optic nerve as a 2 mm-radius cylinder emerging from the posterior globe (Fig. 1).

The tumor was modeled as an oval-shaped lesion at the posterior pole beneath the plaque, defined geometrically as the intersection of the globe with a virtual oval volume with a variable

radius in the z-axis. Since the same lateral size was used for all tumor heights, a variable-size oval intersecting a fixed 12 mm globe produces a fixed lateral but a different depth. Seven tumor apical heights were simulated: 4, 5, 6, 7, 8, 10, and 12 mm. The tumor base (radius ~7 mm) was conformal with the scleral curvature, and the tumor apex was aligned with the plaque central axis.

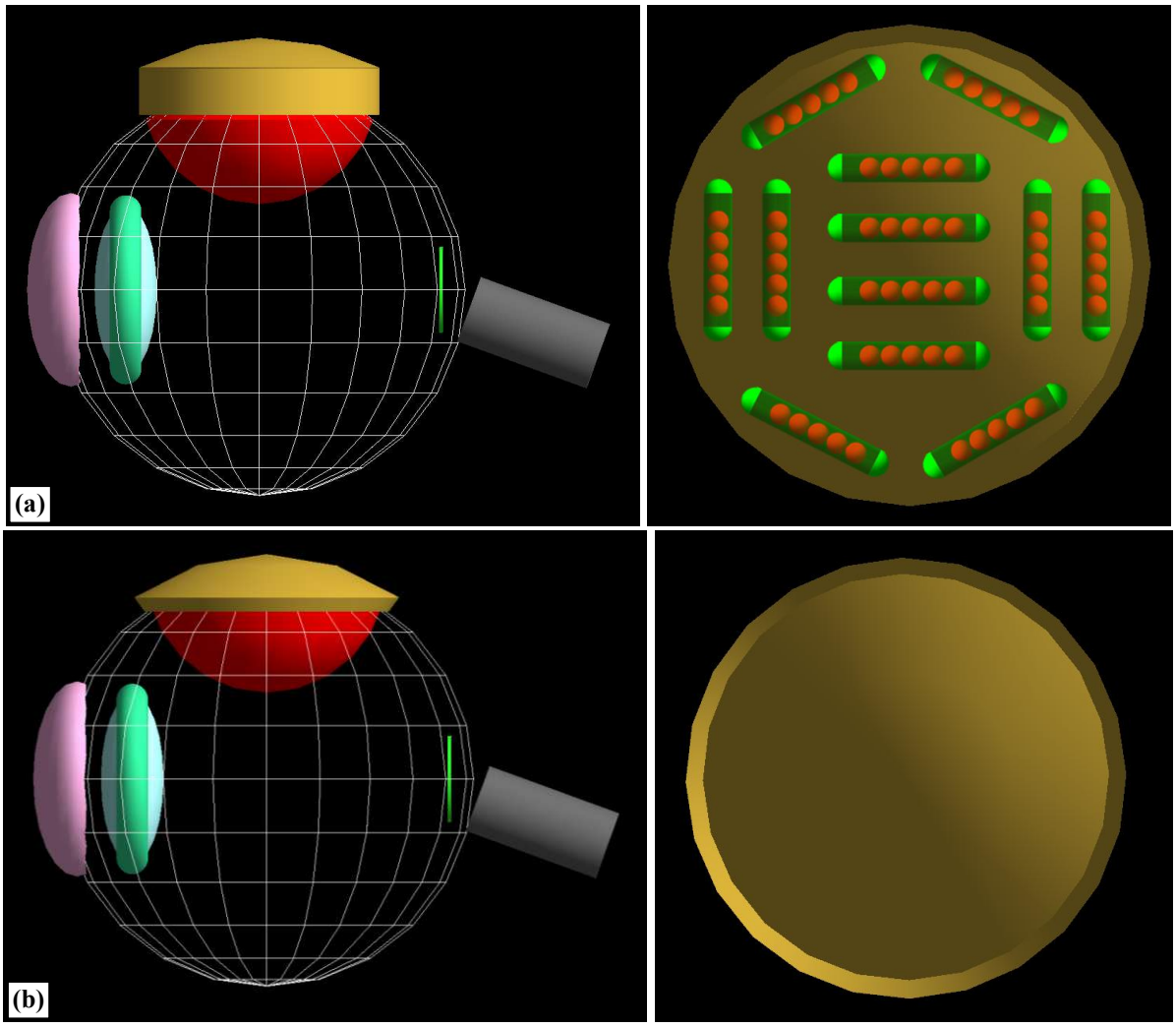


Fig. 1 Schematic representation of the simulated eye phantom with its radiosensitive organs as well as the simulated radioactive eye plaques: **(a)** COMS ^{125}I and **(b)** CCA ^{106}Ru

2.5. Source verification and DVH analysis

2.5.1. Verification of the simulated sources

Both plaque models were verified against independent data before being used for the comparative DVH analysis. For each plaque, simulated depth-dose curves along the plaque central axis were compared with published measurements, e.g., data obtained using EBT3 radiochromic film for CCA-type plaques [7]. The central axis of the plaque was voxelized (with 0.5 mm size) up to a depth of 1 cm along the (z-axis) to obtain the depth-dose profile. The dose reference point was determined at 2-mm depth on the central axis of the plaque.

For the ^{125}I seed verification, the Imagyn IS-12501 model was previously validated against the AAPM TG-43 dosimetry protocol in a prostate brachytherapy geometry using the identical source geometry and spectral definition [20], where calculated dose rate constant, radial dose functions and anisotropy functions agreed with TG-43 consensus data within 3%.

2.5.2. Dose scoring and DVH computation

Dose was scored on a voxelized mesh as a structure-conformal mesh over which the tumor and each organ at risk were segmented. Structures included in the DVH analysis were the tumor and the adjacent OAR: optic nerve, lens, and cornea. Dose was scored using *DoseToMedium* module of TOPAS. Cumulative DVHs were constructed with different dose bins using *CumulativeVolumeHistogram* module of TOPAS, and all DVH metrics were extracted from the cumulative distribution by linear interpolation between bin centers. The number of dose bins was 256, 384, 512, 640, and 768 for the 4, 6, 8, 10, and 12 mm tumor. The number of dose bins for optic nerve, lens, and cornea was 64, 108, and 500 for all tumor sizes.

Each plaque was independently normalized so that the absorbed dose at 4 mm depth on the plaque central axis was 85 Gy. This fixed-depth reference was chosen because it is approximately the COMS prescription dose at the apex of a small-to-medium tumor, and because it is physically achievable by both plaque types; an apex-based prescription at 85 Gy is not achievable by the ^{106}Ru plaque for apical heights beyond approximately 6 mm. Under this normalization, both plaques deliver an identical dose at a common reference depth, so that differences at all other depths and in all other structures reflect the intrinsic dose-gradient characteristics of each source. Because the 85 Gy isodose surface passes through the same geometric point for both plaques, V_{85Gy} is largely determined by tumor geometry rather than by plaque type, and it is reported as a normalization check rather than as a discriminative dosimetric endpoint. Coverage at a sub-prescription threshold, $V_{42.5Gy}$ (50% of the reference dose), is reported as the discriminative coverage metric, alongside apex dose (D_{min}), D_{98}, and the D_{50}/D_{98} heterogeneity ratio.

Tumor dose homogeneity was quantified using the ICRU Report 83 homogeneity index, $HI = (D_2 - D_{98})/D_{50}$, where D_n is the dose received by n% of the target volume. Lower values indicate greater homogeneity. Because HI is a D_{50}-normalized relative index developed for external-beam photon therapy, and because eye-plaque brachytherapy produces steep dose gradients across the target, HI is reported here for comparability with the literature and is interpreted alongside absolute coverage metrics, D_{95} (Gy), V_{85}Gy (%).

For each OAR, the following metrics were extracted from the cumulative DVHs: D_{max}, D_{min}, D_{mean}, and the volume metrics V_{1Gy}, V_{2Gy}, V_{10Gy}, and V_{20Gy} defined as the percentage of the structure volume receiving at least 1, 2, 10, and 20 Gy, respectively.

All simulations were run with 2.147×10^9 primary particles on a 40-thread CPU system with 80 GB of RAM. Statistical uncertainty in scored dose was below 0.5% within the tumor volume and below 2% in the most distant organ at risk, the optic nerve.

3. Result

Central-axis percent depth-dose (PDD) curves calculated with TOPAS for the ^{125}I COMS and ^{106}Ru CCA plaques are compared with reference data in Fig 2. Dose was normalized to 100%

at a depth of 2 mm on the plaque central axis for both plaque types. Error bars in Fig. 2 denote ±5% of the plotted value as the simulation uncertainty.

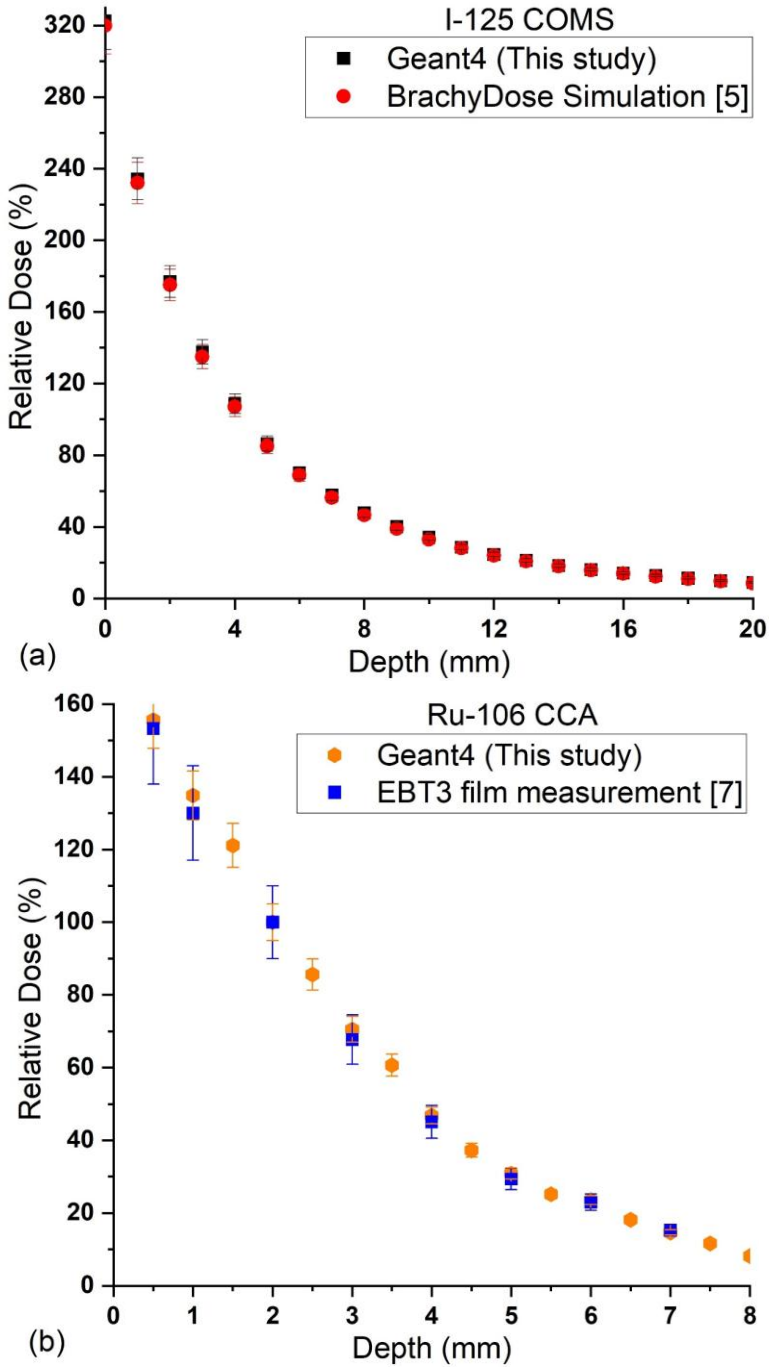


Fig. 2 Comparison of percent depth dose of I-125 COMS **(a)** and Ru-106 CCA **(b)** plaques obtained by TOPAS in this study with the experimental data [5, 7]. Dose values are normalized to 100% at a depth of 2 mm on the central axis

For the ^{106}Ru CCA plaque, the calculated PDD agreed with the EBT3 radiochromic film measurements of reference [7] to within 5% over the 0–7 mm range, with a maximum local difference of 4.96% at 5 mm. For the ^{125}I COMS plaque, the calculated PDD agreed with the reference data of Ref. [5] to within 5% over the 0–20 mm range, with a maximum local difference of 4.95% at 17 mm.

Cumulative DVHs for the tumor and the three reported OAR (lens, cornea, and optic nerve) are shown in Figs. 3–9 for tumor apical heights of 4, 5, 6, 7, 8, 10, and 12 mm, respectively. Panels (a) and (b) in each figure correspond to the ^{125}I COMS and ^{106}Ru CCA plaques.

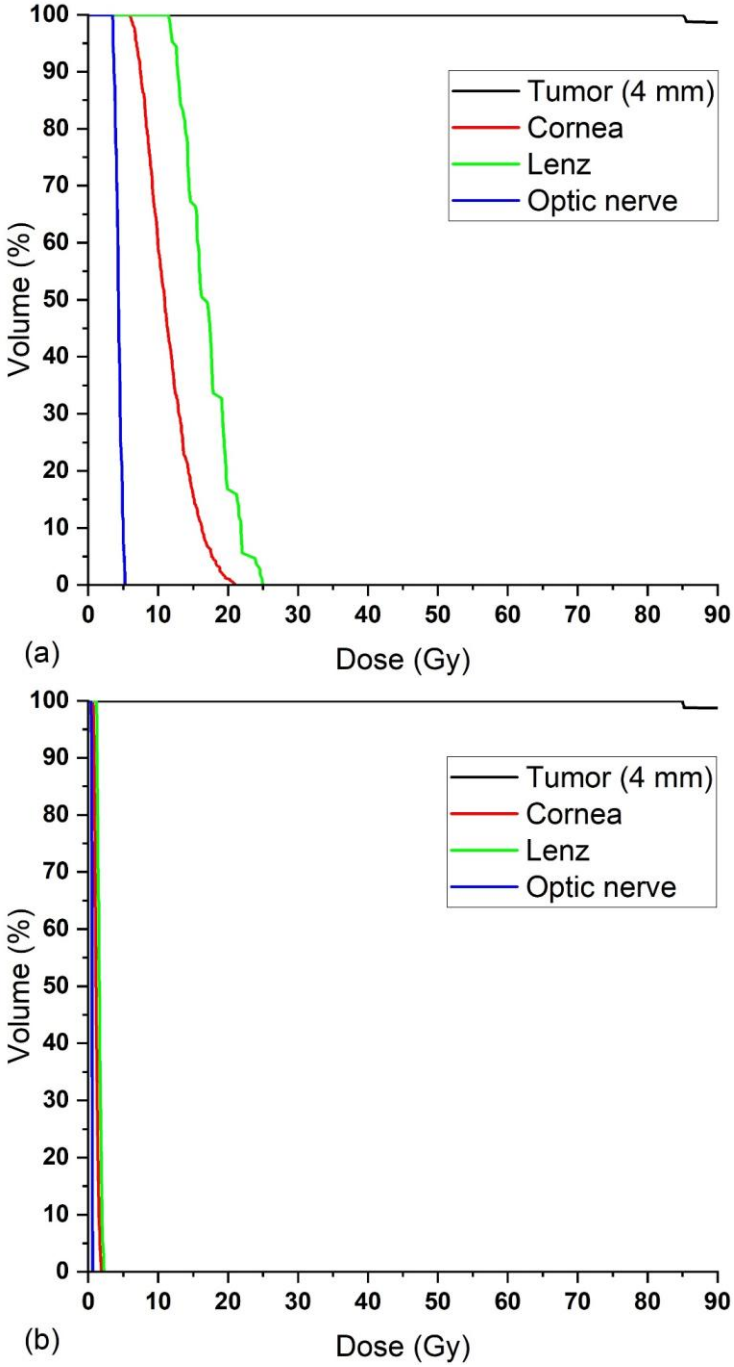


Fig. 3 Dose volume histograms (DVHs) of the tumor, Lens, cornea, and optic nerve for the **(a)** ^{125}I and **(b)** ^{106}Ru plaques for a 4-mm deep tumor

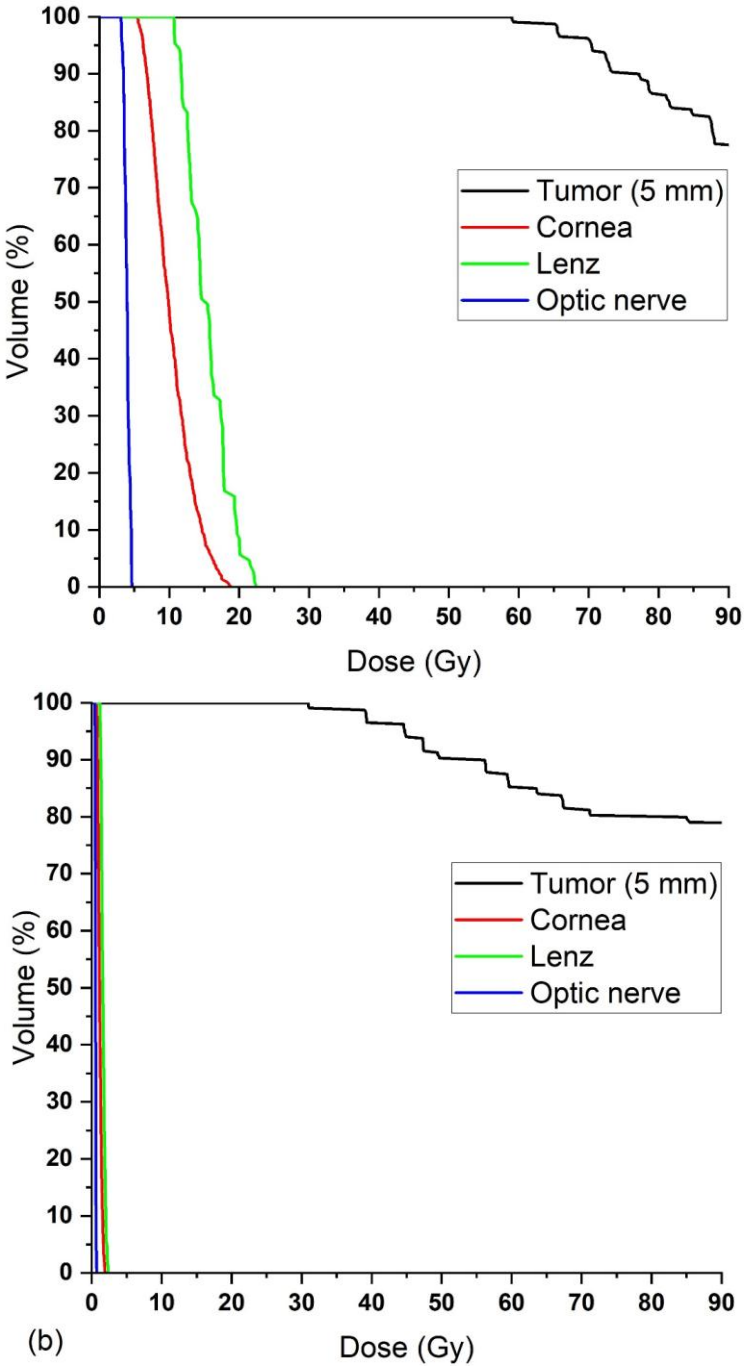


Fig. 4 Dose volume histograms (DVHs) of the tumor, Lens, cornea, and optic nerve for the **(a)** ^{125}I and **(b)** ^{106}Ru plaques for a 5-mm deep tumor

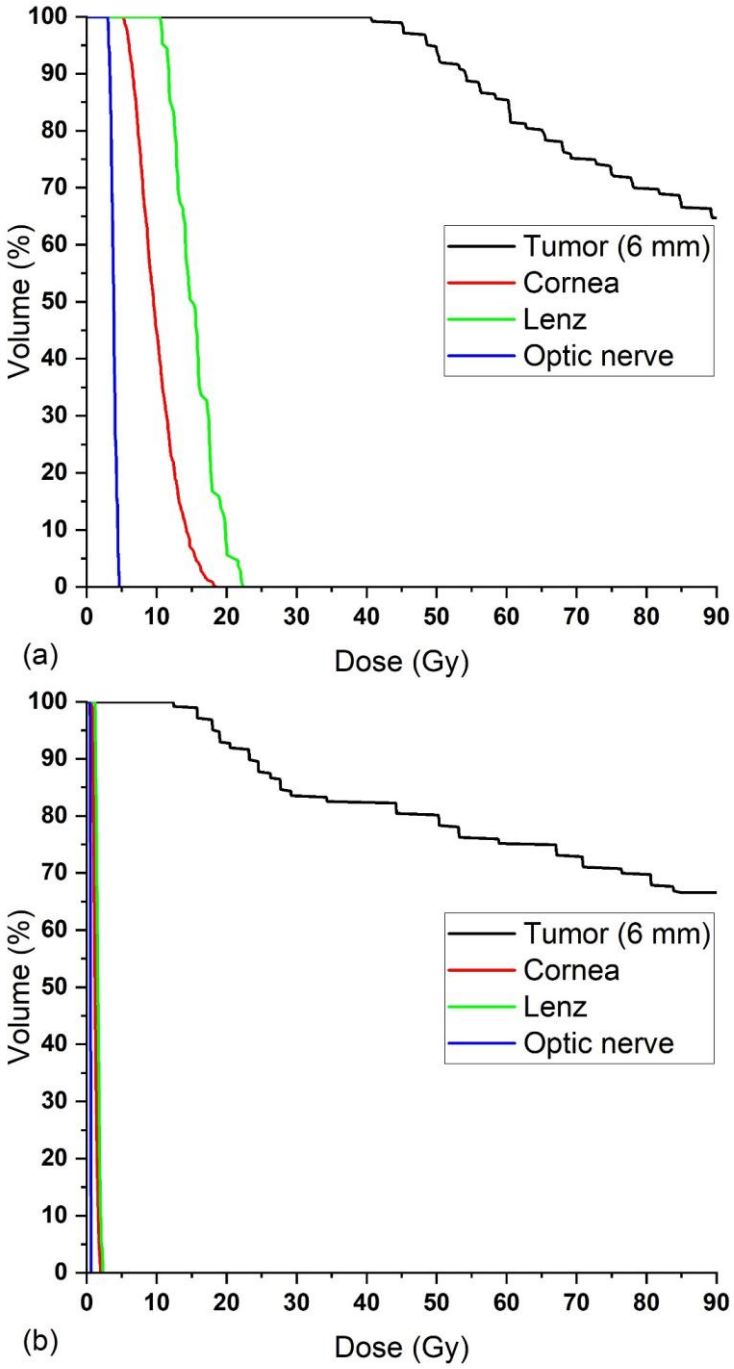


Fig. 5 Dose volume histograms (DVHs) of the tumor, Lens, cornea, and optic nerve for the **(a)** ^{125}I and **(b)** ^{106}Ru plaques for a 6-mm deep tumor

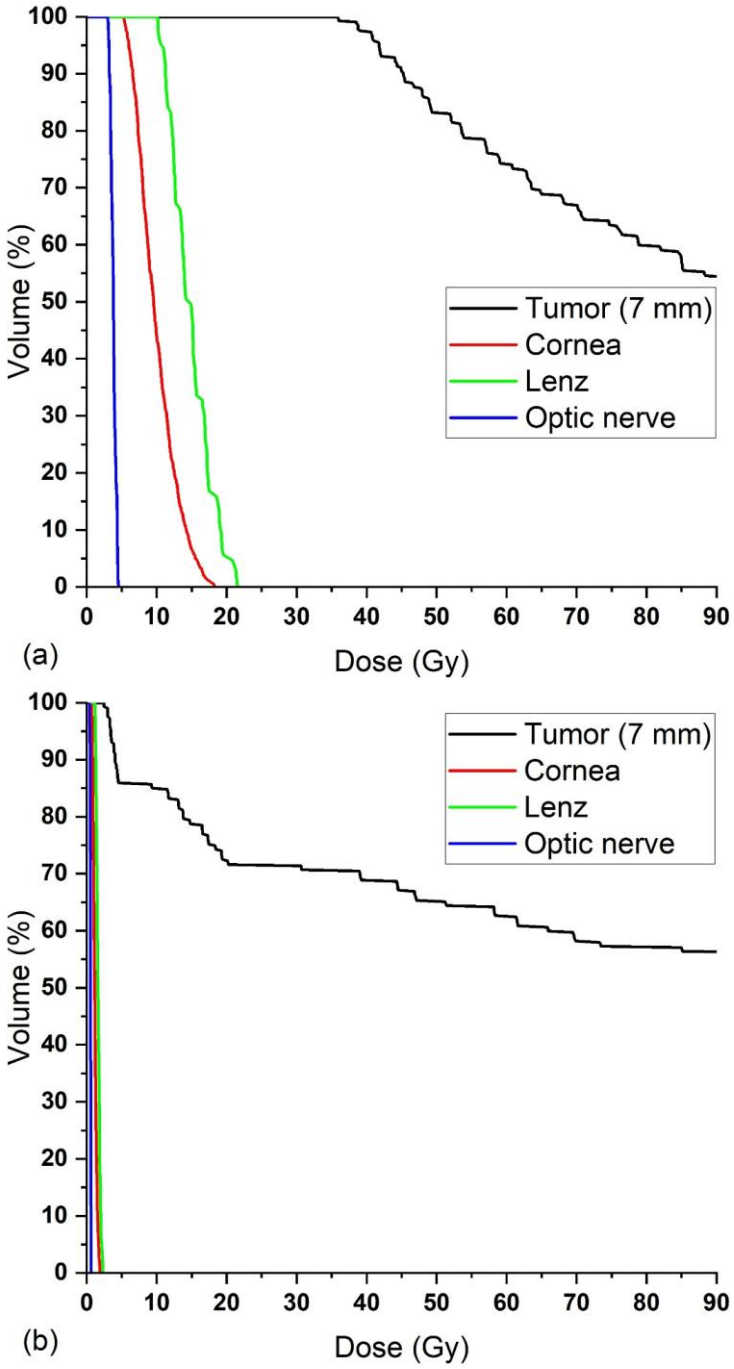


Fig. 6 Dose volume histograms (DVHs) of the tumor, Lens, cornea, and optic nerve for the **(a)** ^{125}I and **(b)** ^{106}Ru plaques for a 7-mm deep tumor

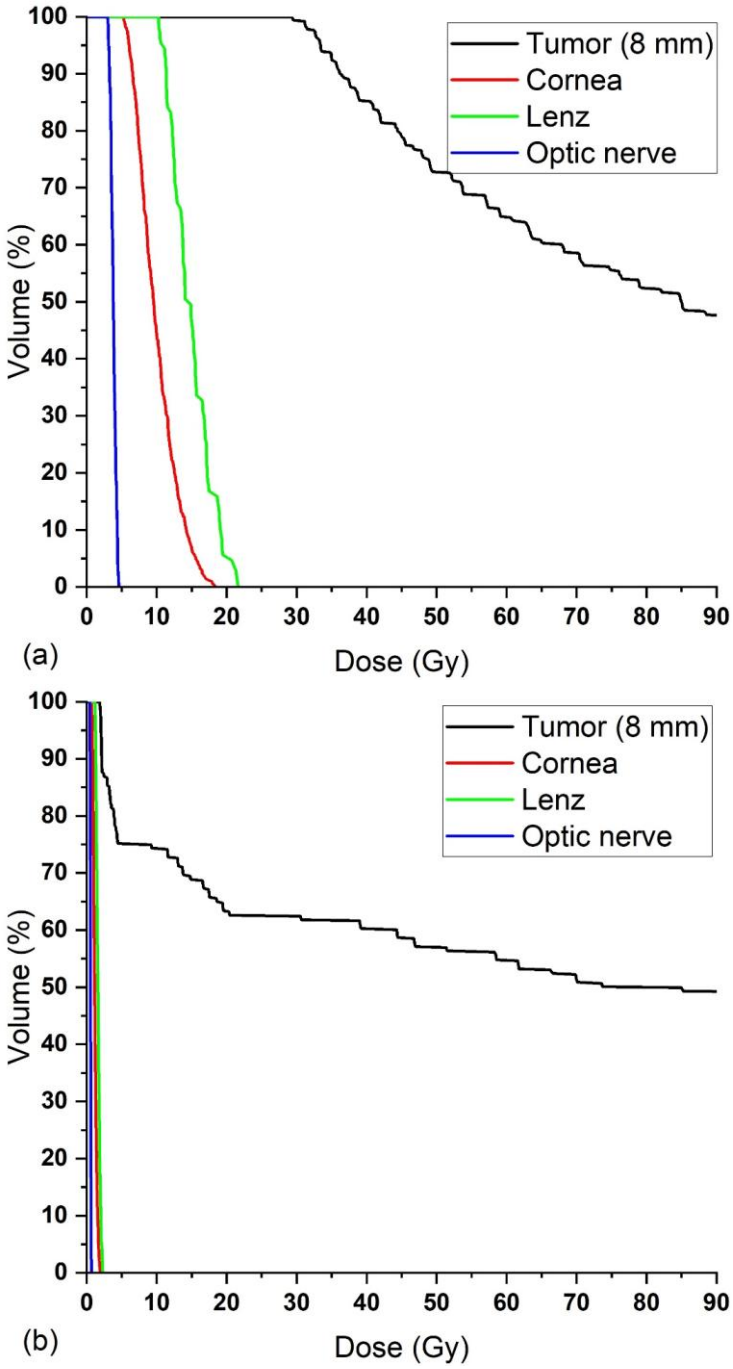


Fig. 7 Dose volume histograms (DVHs) of the tumor, Lens, cornea, and optic nerve for the **(a)** ^{125}I and **(b)** ^{106}Ru plaques for an 8-mm deep tumor

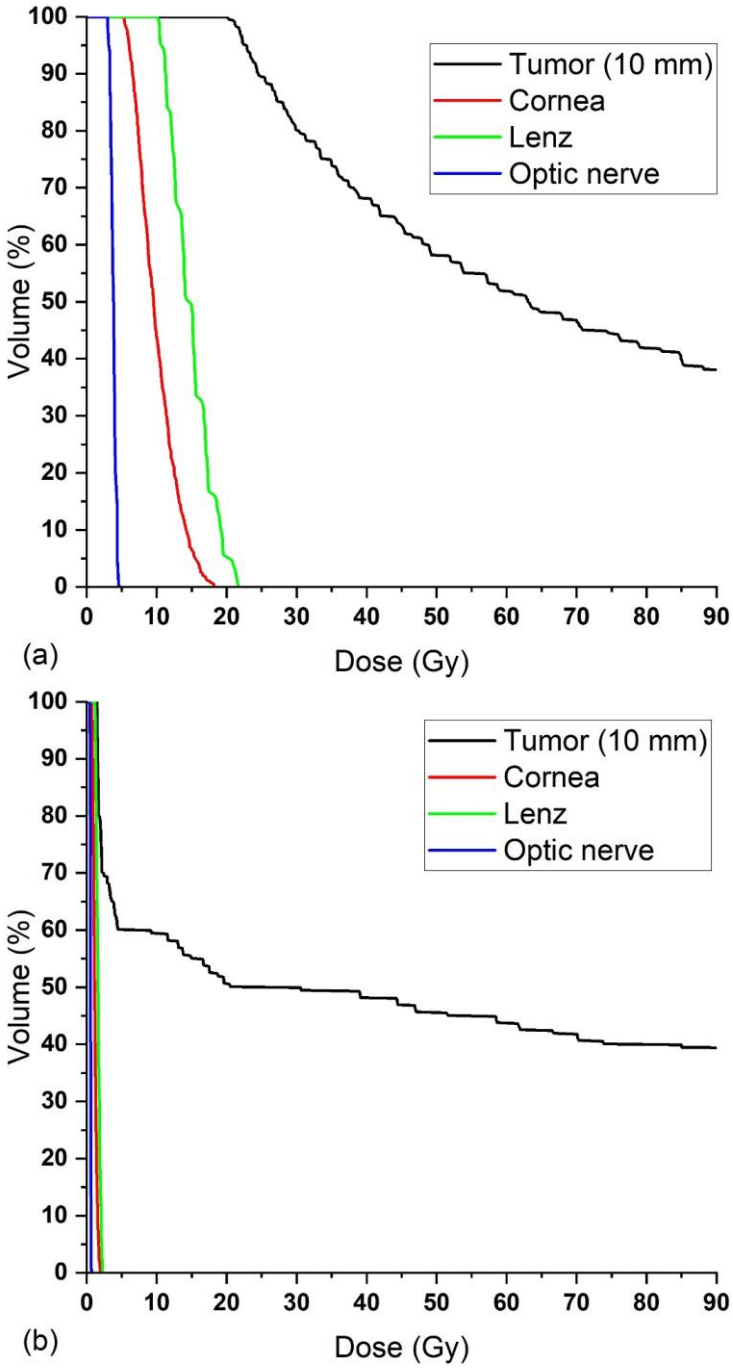


Fig. 8 Dose volume histograms (DVHs) of the tumor, Lens, cornea, and optic nerve for the **(a)** ^{125}I and **(b)** ^{106}Ru plaques for a 10-mm deep tumor

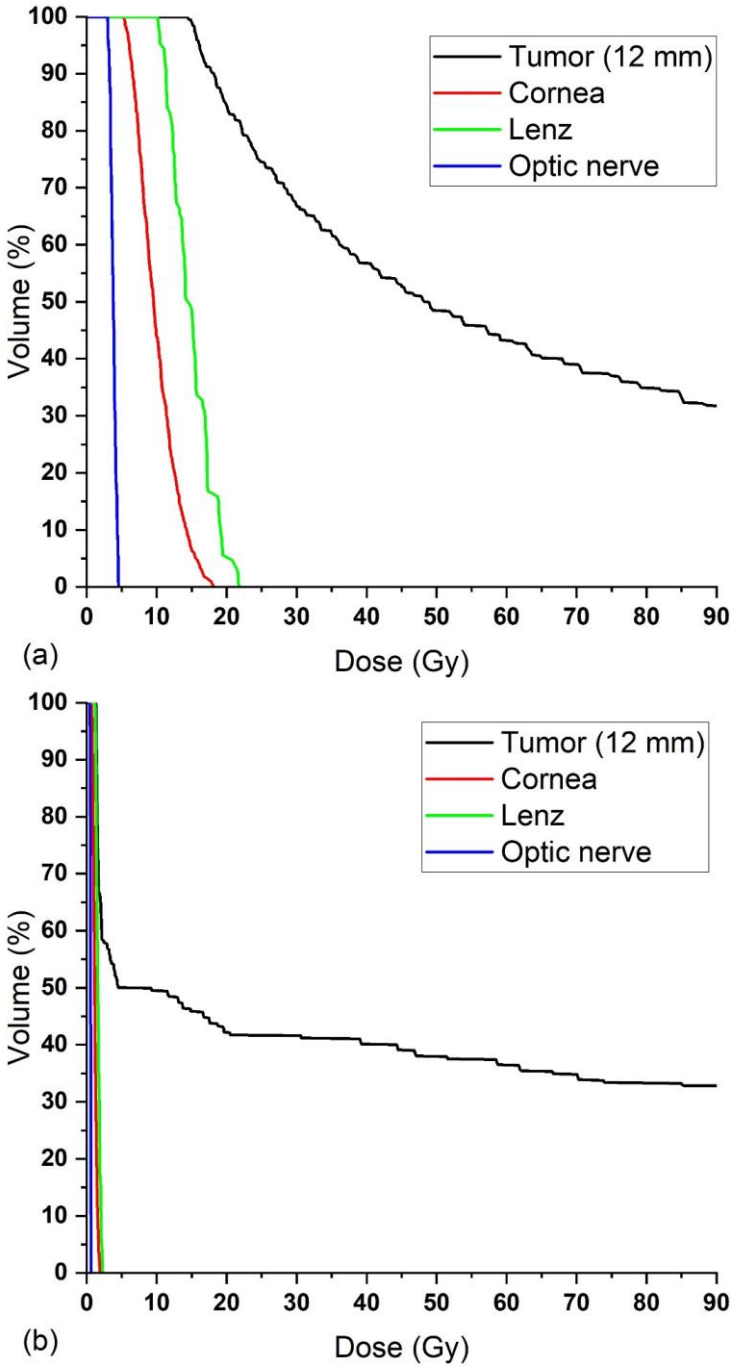


Fig. 9 Dose volume histograms (DVHs) of the tumor, Lens, cornea, and optic nerve for the **(a)** ^{125}I and **(b)** ^{106}Ru plaques for a 12-mm deep tumor

Tumor DVH metrics for I-125 and Ru-106 plaque types at all seven tumor heights are summarized in Tables 1 and 2, respectively.

Table 1. Tumor dosimetric parameters for the ^{125}I eye plaque as a function of tumor apical height. All values are derived from cumulative DVHs after normalization to 85 Gy at the 4-mm depth.

	Tumor Depth

DVH Parameter	4 mm	5 mm	6 mm	7 mm	8 mm	10 mm	12 mm
Dmax (Gy)	717.6	649.39	628.05	627.67	629.1	628.11	629.58
Dmin (Gy)	85.0	59.01	40.578	35.838	29.251	20.031	14.333
Dmean (Gy)	287.4	223.33	218.3	168.49	151.92	126.4	108.36
D98 (Gy)	96.726	65.479	45.23	38.769	31.464	21.768	15.377
D90 (Gy)	109.21	77.22	54.1	45.25	36.181	24.53	18.22
D50 (Gy)	202.71	151.9	135.3	97.191	84.958	63.042	48.168
D2 (Gy)	701.24	634.01	615.26	613.35	612.63	600.07	577.02
HI	2.98	3.74	4.21	5.91	6.84	9.17	11.6
V_{85Gy} (%)	100	82.76	66.58	57.05	49.90	39.90	33.25
$V_{42.5Gy}$ (%)	100	100	99.1	92.9	81.3	65.02	54.17

Table 2. Tumor dosimetric parameters for the ^{106}Ru eye plaque as a function of tumor apical height. All values are derived from cumulative DVHs after normalization to 85 Gy at the 4-mm depth.

DVH Parameter	Tumor Depth						
	4 mm	5 mm	6 mm	7 mm	8 mm	10 mm	12 mm
Dmax (Gy)	3700.9	3725.28	3726.54	3746.36	3744.73	3750.05	3753.41
Dmin (Gy)	85.0	30.93	12.36	2.467	1.855	1.266	1.041
Dmean (Gy)	1164.3	948.9	752.0	684.8	599.3	480.4	400.85
D98 (Gy)	108.96	39.2	15.798	2.99	1.958	1.299	1.061
D90 (Gy)	131.85	52.93	23.233	4.062	2.151	1.368	1.12
D50 (Gy)	502.83	390.9	282.2	157.2	79.4	25.54	6.86
D2 (Gy)	3664.25	3687.98	3701.1	3707.8	3706.8	3676.76	3633.6
HI	7.10	9.33	13.1	23.5	46.6	143.9	529.4
V_{85Gy} (%)	100	79.94	66.58	57.05	49.9	39.9	33.24
$V_{42.5Gy}$ (%)	100	96.4	82.5	68.9	60.1	48.1	40.1

OAR DVH metrics are summarized in Table 3 for the ^{125}I COMS plaque and in Table 4 for the ^{106}Ru CCA plaque.

Table 3. Organ-at-risk dosimetric parameters for the ^{125}I COMS eye plaque as a function of tumor apical height. V_{nGy} denotes the percentage of structure volume receiving at least n Gy in %.

OAR	DVH Parameter	Tumor Depth						
		4 mm	5 mm	6 mm	7 mm	8 mm	10 mm	12 mm
Cornea	Dmax (Gy)	21.095	18.895	18.59	18.39	18.47	18.245	18.201
	Dmin (Gy)	5.917	5.404	5.206	5.192	5.169	5.144	5.123
	Dmean (Gy)	11.42	10.34	10.03	10.02	10.02	10.01	10.0
	V_{1Gy} (%)	100	100	100	100	100	100	100
	V_{2Gy} (%)	100	100	100	100	100	100	100
	V_{5Gy} (%)	100	100	100	100	100	100	100

	$V_{8.5Gy}$ (%)	79.2	66.9	64.5	63.9	63.9	63.9	63.7
	V_{10Gy} (%)	59.3	48.5	44.7	44.1	44.1	44.1	43.7
	V_{20Gy} (%)	1.20	0	0	0	0	0	0
Lens	Dmax (Gy)	24.938	22.453	22.34	21.528	21.674	21.701	21.755
	Dmin (Gy)	11.45	10.683	10.42	10.12	10.26	10.103	10.091
	Dmean (Gy)	17.0	15.42	15.38	14.88	14.9	14.89	14.92
	V_{1Gy} (%)	100	100	100	100	100	100	100
	V_{2Gy} (%)	100	100	100	100	100	100	100
	V_{5Gy} (%)	100	100	100	100	100	100	100
	$V_{8.5Gy}$ (%)	100	100	100	100	100	100	100
	V_{10Gy} (%)	100	100	100	100	100	100	100
	V_{20Gy} (%)	16.8	9.34	7.47	5.61	5.61	5.61	5.61
Optic nerve	Dmax (Gy)	5.265	4.664	4.583	4.535	4.583	4.578	4.552
	Dmin (Gy)	3.515	3.106	3.035	3.026	2.967	2.998	3.006
	Dmean (Gy)	4.351	3.94	3.82	3.81	3.8	3.8	3.8
	V_{1Gy} (%)	100	100	100	100	100	100	100
	V_{2Gy} (%)	100	100	100	100	100	100	100
	V_{5Gy} (%)	12.7	0	0	0	0	0	0
	$V_{8.5Gy}$ (%)	0	0	0	0	0	0	0
	V_{10Gy} (%)	0	0	0	0	0	0	0
	V_{20Gy} (%)	0	0	0	0	0	0	0

297

Table 4. Organ-at-risk dosimetric parameters for the ^{106}Ru CCA eye plaque as a function of tumor apical height. V_{nGy} denotes the percentage of structure volume receiving at least n Gy in %.

298
299
300

OAR	DVH Parameter	Tumor Depth						
		4 mm	5 mm	6 mm	7 mm	8 mm	10 mm	12 mm
Cornea	Dmax (Gy)	1.945	1.974	1.982	1.935	1.943	1.99	1.963
	Dmin (Gy)	0.665	0.676	0.692	0.681	0.691	0.664	0.682
	Dmean (Gy)	1.159	1.166	1.232	1.174	1.177	1.174	1.179
	V_{1Gy} (%)	67.73	67.33	76.35	70.74	68.53	69.74	69.75
	V_{2Gy} (%)	0	0	0	0	0	0	0
	V_{5Gy} (%)	0	0	0	0	0	0	0
	V_{10Gy} (%)	0	0	0	0	0	0	0
	V_{20Gy} (%)	0	0	0	0	0	0	0
Lens	Dmax (Gy)	2.306	2.355	2.3048	2.3056	2.302	2.256	2.284
	Dmin (Gy)	1.139	1.172	1.185	1.1196	1.172	1.152	1.14
	Dmean (Gy)	1.607	1.631	1.63	1.637	1.631	1.641	1.637
	V_{1Gy} (%)	100	100	100	100	100	100	100
	V_{2Gy} (%)	8.41	12.15	9.34	11.21	12.14	14.01	15.89
	V_{5Gy} (%)	0	0	0	0	0	0	0
	V_{10Gy} (%)	0	0	0	0	0	0	0

	V_{20Gy} (%)	0	0	0	0	0	0	0
Optic nerve	Dmax (Gy)	0.6376	0.7146	0.6516	0.6442	0.662	0.673	0.654
	Dmin (Gy)	0.4148	0.451	0.4462	0.3982	0.436	0.439	0.435
	Dmean (Gy)	0.548	0.552	0.552	0.55	0.553	0.552	0.56
	V_{1Gy} (%)	0	0	0	0	0	0	0
	V_{2Gy} (%)	0	0	0	0	0	0	0
	V_{5Gy} (%)	0	0	0	0	0	0	0
	V_{10Gy} (%)	0	0	0	0	0	0	0
	V_{20Gy} (%)	0	0	0	0	0	0	0

Fig. 10 shows the D50/D98 ratio for both plaque types at all seven tumor heights.

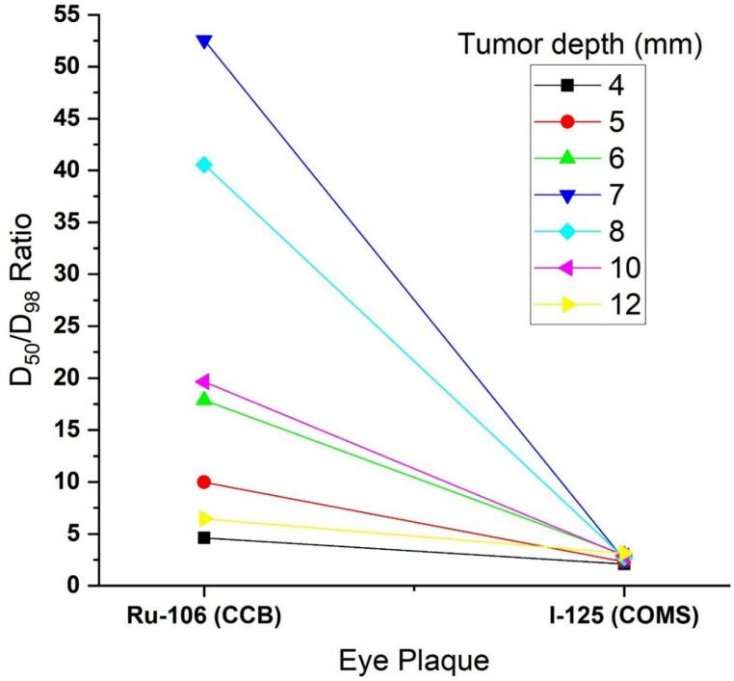


Fig. 10 The D50/D98 ratio for I-125 and Ru-106 plaque types at all tumor heights of 4-12 mm

4. Discussion

4.1 Principal findings

This study compared the dose-volume characteristics of a photon-emitting ^{125}I COMS plaque and a beta-emitting ^{106}Ru CCA plaque across seven tumor apical heights (4–12 mm) under a common normalization of 85 Gy at 4 mm depth. Four findings emerge.

First, as showing in Figs. 2-9, the two plaque types produced qualitatively different intratumoral dose distributions rather than differing merely in penetration depth. According to Tables 11 and 2, the ^{106}Ru plaque delivered a higher median tumor dose than ^{125}I at every height up to 7 mm (502.8 vs 202.7 Gy at 4 mm; 157.2 vs 97.2 Gy at 7 mm), yet its dose to the tumor apex was

lower than that of ^{125}I at every height beyond 4 mm, by factors of 1.9 at 5 mm, 3.3 at 6 mm, and 14.5 at 7 mm, reaching 15.8 at 8 mm and 13.8 at 12 mm.

Second, the conclusion of the comparison depends on which DVH metric is used. By median dose, the beta plaque appeared superior through approximately 7.8 mm, where the two D_{50} curves crossed. By apex dose, D_{98}, or $V_{42.5Gy}$, the photon plaque was equal or superior at every tumor height, with no crossover at any height. This metric dependence is, in our view, the most consequential result of the study, and it has direct implications for how plaque comparisons should be reported.

Third, intratumoral heterogeneity diverged by more than an order of magnitude, and the divergence was depth-specific rather than monotonic. As shown in Fig. 10, the ^{106}Ru D_{50}/D_{98} ratio rose from 4.62 at 4 mm to a maximum of 52.6 at 7 mm, whereas the ^{125}I ratio remained between 2.10 and 3.13 across the entire range. The maximum heterogeneity of the beta plaque coincided with the tumor height at which the choice between plaque types becomes clinically consequential.

Fourth, as listed in Tables 1-4, OAR doses were approximately one order of magnitude lower for ^{106}Ru than for ^{125}I (lens D_{mean} 1.61–1.64 vs 14.88–17.0 Gy; cornea 1.16–1.23 vs 10.0–11.4 Gy; optic nerve 0.55–0.56 vs 3.80–4.35 Gy) and were essentially independent of tumor height for both plaques, a structural consequence of the fixed plaque-to-sclera geometry of the phantom.

4.2 Metric dependence

Under independent normalization to 85 Gy at 4 mm, V_{85}Gy was 100% at 4 mm and declined almost identically for both plaques at greater heights (82.76% vs 79.94% at 5 mm; 66.58% for both at 6 mm; 57.05% for both at 7 mm; 49.90% vs 49.90% at 8 mm). This identity is not a coincidental similarity between two dose distributions; it is a geometric necessity of the normalization. The 85 Gy isodose surface passes through the same physical point, 4 mm depth on the central axis, for both plaques, and the fraction of a lens-shaped tumor lying proximal to a plane at a fixed fractional height is determined by tumor geometry, not by the source. Beyond approximately 6 mm, where the 4 mm plane lies well inside the tumor, the two plaques are indistinguishable by V_{85Gy}.

This has a methodological implication that extends beyond the present comparison. A single coverage metric evaluated at the normalization dose cannot discriminate between two sources normalized to that dose. Discrimination requires metrics evaluated at doses or depths other than the reference. In the present data, three such metrics are available: apex dose (D_{min}), the near-minimum dose D_{98}, and coverage at half the reference dose ($V_{42.5Gy}$). $V_{42.5Gy}$ is the most transparent of these because it is anchored to an explicit sub-prescription threshold: the ^{125}I values exceeded the ^{106}Ru values at every height beyond 4 mm, and the gap widened from 0.9 percentage points at 6 mm (99.1% vs 82.5%) to 24.0 points at 7 mm (92.9% vs 68.9%), remaining above 14 points through 12 mm.

It is therefore recommended that comparative plaque dosimetry report at least one sub-prescription coverage threshold and the near-minimum dose alongside any prescription-dose coverage metric. Reporting V_{85Gy} alone would have led to the incorrect conclusion that the two plaques are dosimetrically equivalent across the clinically relevant depth range.

4.3 Physical basis of the divergent distributions

The observed divergence is a direct consequence of the different energy-deposition physics of beta particles and low-energy photons.

For a beta emitter, the dose distribution is dominated by short-range electrons whose fluence attenuates approximately exponentially with depth. The ^{106}Rh beta endpoint of 3.54 MeV corresponds to a continuous slowing-down range in water of roughly 15 mm and a practical range of approximately 10–12 mm; however, the *spectrum-averaged* attenuation is far steeper, because the low-energy component of the beta spectrum is absorbed within the first few millimeters. The result is a dose distribution that is intense but shallow: a very high surface dose, a steep fall-off, and an effective range beyond which the dose collapses to near zero. In the present data this appears as a D_{max} of approximately 3,700 Gy against a 4 mm reference dose of 85 Gy, a surface-to-reference ratio of 43.5, and as a D_{98} that falls below 3 Gy by 7 mm.

For a low-energy photon emitter, the dose distribution is determined by photon attenuation and by scatter buildup in the irradiated volume. The ^{125}I spectrum (mean ~28 keV) attenuates approximately exponentially in the absence of scatter, but scattered photons redistribute dose into the deeper volume and produce a broad, gradually declining distribution. In the present data this appears as a D_{max} of only 628–718 Gy against a reference of 85 Gy, a surface-to-reference ratio of 7.4–8.5, roughly fivefold lower than for the beta plaque, and as a D_{98} that declines only from 96.7 to 15.4 Gy across the full 4–12 mm range.

The consequence is the hot-bulk/cold-apex partition described in section 4.1: the beta plaque concentrates dose in the tumor volume proximal to the source and leaves the distal volume essentially unirradiated, whereas the photon plaque distributes dose more uniformly across the target at the cost of higher dose to everything else. This is not a difference in "penetration" as a scalar property; it is a difference in the *shape* of the dose distribution, and it is captured by the D_{50}/D_{98} ratio but not by D_{50} or D_{mean} alone.

The same physics explains why D_{mean} is an unreliable descriptor for beta plaques at depth. At 12 mm, the ^{106}Ru D_{mean} was 400.85 Gy against a D_{50} of 6.86 Gy, a mean-to-median ratio of 58.4, compared with 2.25 for ^{125}I. The beta plaque's mean dose is determined by a thin layer of very-high-dose surface voxels and describes no voxel in the tumor. Reporting D_{mean} without D_{50} or D_{98} would therefore substantially overstate the dose delivered to the target by a beta-emitting plaque.

4.5 Depth-stratified plaque selection

According to Fig. 10, the ^{106}Ru D_{50}/D_{98} ratio peaked at 52.6 at 7 mm and declined to 40.6, 19.7, and 6.46 at 8, 10, and 12 mm. This decline should not be interpreted as improving homogeneity. Beyond 7 mm both the numerator and the denominator collapse toward the dose floor: at 12 mm, D_{50} was 6.86 Gy and D_{98} was 1.06 Gy, a ratio of 6.46 between two doses that are both therapeutically negligible. The ratio falls because the two metrics are being divided as both approach zero, not because the distribution becomes more uniform. The correct reading of the curve is that beta-plaque heterogeneity *saturates* beyond 7 mm in a regime where the target is no longer meaningfully irradiated, and the peak at 7 mm marks the transition between "heterogeneous but partly treated" and "effectively untreated."

It is stated explicitly because a reader who interprets the declining right limb of the curve as a return toward homogeneity would draw the opposite conclusion to the one the data support.

Taken together, the data support a depth-stratified selection rule based on the metric that is appropriate to the clinical question, rather than on a single global preference for one plaque type.

Tumors of approximately 4 mm apical height are treated to the reference dose by both plaques by construction, and the dosimetric comparison is uninformative at exactly this depth. The choice is therefore governed by considerations outside the present analysis: OAR dose, which favors ^{106}Ru by approximately one order of magnitude; availability; and the treating center's experience.

Tumors of 5–6 mm apical height represent the transition zone. The ^{106}Ru plaque still delivers a higher median dose (390.9 vs 151.9 Gy at 5 mm; 282.2 vs 135.3 Gy at 6 mm) but its apex dose has already fallen to 30.9 and 12.4 Gy, corresponding to 36% and 15% of the reference, and its D_{98} to 39.2 and 15.8 Gy. The ^{125}I plaque maintains apex doses of 59.0 and 40.6 Gy and D_{98} values of 65.5 and 45.2 Gy. Whether this degree of apical underdosing is acceptable is a clinical judgment that the present dosimetric analysis cannot resolve, but the data quantify the trade-off explicitly.

Tumors of 7 mm and above show a clear divergence. The ^{106}Ru apex dose falls below 5% of the reference between 6 and 7 mm and reaches 1.04 Gy at 12 mm, while the ^{125}I apex dose declines only to 14.3 Gy. No plausible radiobiological correction can convert 1–3 Gy to a tumoricidal dose, whereas a 14–36 Gy apex dose, although below the prescription, may carry meaningful biological effect depending on the alpha/beta ratio and the dose rate. For tumors of this depth, the data support ^{125}I as the dosimetrically appropriate choice.

The crossover at approximately 7.8 mm in the D_{50} curves is therefore a crossover in a metric that should not drive plaque selection. The clinically decisive transition occurs between 5 and 7 mm, and it is visible only in the apex-dose and near-minimum-dose metrics.

4.6 OAR sparing and its limits

The approximately tenfold reduction in OAR dose with the ^{106}Ru plaque is the most robust and least metric-dependent result of this study. Because the plaque position is fixed relative to the sclera, OAR doses were essentially invariant with tumor height for both plaques (for ^{125}I, lens D_{mean} varied by 14% across seven heights; for ^{106}Ru, by 2%). This invariance simplifies the clinical argument considerably: the OAR comparison is a constant offset in favor of the beta plaque, and the choice between plaque types is therefore driven entirely by target coverage rather than by a depth-dependent trade-off between target and normal tissue.

Two caveats limit this conclusion. First, the phantom geometry placed the plaque at a fixed position relative to the sclera and did not model plaque tilt, eccentric tumor location, or peripapillary or macular tumors, all of which would alter the plaque-to-OAR distances and hence the sparing observed here. Second, the D_{max} of approximately 3,700 Gy for the ^{106}Ru plaque at the source-adjacent surface reflects the extreme steepness of the beta gradient and, although it is a single-voxel value adjacent to the source window, it indicates that the scleral surface dose under any normalization delivering 85 Gy at 4 mm is far above reported scleral tolerance thresholds. Scleral necrosis is a recognized complication of ^{106}Ru plaque therapy, and

the present data are consistent with a scleral-dose constraint being an additional limitation on beta-plaque prescription at depth. Scleral dose should be reported explicitly in future comparative work.

4.7 Limitations

Several limitations should be acknowledged.

Normalization and prescription. Both plaques were normalized to 85 Gy at 4 mm depth rather than prescribed to the tumor apex. This choice was necessary because apex-based prescription at 85 Gy is not physically achievable by the ^{106}Ru plaque at heights beyond approximately 6 mm, and because a fixed-depth reference isolates the effect of source physics from the effect of prescription convention. It does mean, however, that the absolute Gy values reported for larger tumors do not correspond to those that would result from a conventional apex-based prescription, and the reported OAR doses scale accordingly. A supplementary analysis using a 2 mm reference or an apex-based prescription for the subset of cases where it is achievable would strengthen the generalizability of the conclusions.

Phantom simplification. The eye phantom used homogeneous ICRP compositions for each ocular structure, a single standardized globe radius of 12 mm, a single plaque position, and an idealized lens-shaped tumor. Inter-patient variation in globe dimensions, plaque tilt, tumor eccentricity, and tumor heterogeneity were not modeled. In particular, tumors located near the equator or the optic disc would have different plaque-to-OAR geometry from the posterior-pole configuration modeled here, and the OAR sparing reported for ^{106}Ru would be expected to vary accordingly.

Structures not analyzed. The phantom included the macula, retina, ciliary body, and iris, but DVH metrics were extracted only for the lens, cornea, and optic nerve. Because radiation maculopathy and retinopathy are among the dominant dose-limiting toxicities in ocular brachytherapy, the absence of macular and retinal DVH data limits the clinical reach of the OAR comparison.

Single realization. One Monte Carlo realization was performed per plaque–tumor-height combination, with statistical uncertainty below 0.5% in the tumor and below 2% in the optic nerve. Voxel-level uncertainty in low-dose regions is higher, and no formal statistical comparison between plaque types was performed; the reported differences are descriptive and should be interpreted against these uncertainty bounds.

Metrics. D_{max} and D_{min} are single-voxel values and are sensitive to scoring voxel size. HI is a D_{50}-normalized relative index.

Radiobiology. RBE, dose rate, and fractionation were not modeled, and no biological or clinical endpoint was evaluated. The conclusions are therefore dosimetric and should not be read as predictions of tumor control or complication probability.

5. Conclusion

Under a common 85 Gy reference at 4 mm depth, the ^{125}I COMS and ^{106}Ru CCA plaques produced qualitatively different intratumoral dose distributions across apical heights of 4–12 mm. The beta-emitting plaque concentrated dose in the tumor bulk, delivering a higher median dose than ^{125}I through 7 mm, but left the apex effectively untreated beyond 5–6 mm; its D_{50}/D_{98}

heterogeneity ratio peaked at 52.6 at 7 mm against 2.5 for ^{125}I. Because the 85 Gy isodose surface passes through the same geometric point for both plaques, prescription-dose coverage (V_{85Gy}) was nearly identical and therefore non-discriminative. Apex dose, D_{98}, and $V_{42.5Gy}$ were discriminative and indicated a dosimetric advantage for ^{125}I at every height beyond 4 mm. The ^{106}Ru plaque reduced mean OAR dose approximately tenfold at all heights, an advantage independent of tumor depth. Plaque selection should therefore be depth-stratified and based on sub-prescription coverage metrics and near-minimum dose rather than on median or mean tumor dose. Comparative plaque dosimetry reporting only prescription-dose coverage may conclude erroneously that the two sources are equivalent.

Reference:

1. Jager MJ, Shields CL, Cebulla CM, Abdel-Rahman MH, Grossniklaus HE, Stern MH et al (2020) Uveal melanoma. Nat Rev Dis Primers 6:24. https://doi.org/10.1038/s41572-020-0158-0
2. Thomson RM, Furutani KM, Kaulich TW, Mourtada F, Rivard MJ, Soares CG et al (2020) AAPM recommendations on medical physics practices for ocular plaque brachytherapy: report of task group 221. Med Phys 47:e92-e124. https://doi.org/10.1002/mp.13996
3. Diener-West M, Earle JD, Fine SL, Hawkins BS, Moy CS, Reynolds SM, Schachat AP, Straatsma BR (2001) The COMS randomized trial of iodine 125 brachytherapy for choroidal melanoma, III: initial mortality findings. COMS Report No. 18. Arch Ophthalmol 119:969-982. https://doi.org/10.1001/archopht.119.7.969
4. Jampol LM, Moy CS, Murray TG, Reynolds SM, Albert DM, Schachat AP, Diddie KR, Engstrom RE, Finger PT, Hovland KR, Joffe L (2020) The COMS randomized trial of iodine 125 brachytherapy for choroidal melanoma: IV. Local treatment failure and enucleation in the first 5 years after brachytherapy. COMS Report No. 19. Ophthalmology 127:S148-S157.
5. Chiu-Tsao ST, Astrahan MA, Finger PT, Followill DS, Meigooni AS, Melhus CS, Mourtada F, Napolitano ME, Nath R, Rivard MJ, Rogers DW, Thomson RM (2012) Dosimetry of (125)I and (103)Pd COMS eye plaques for intraocular tumors: report of Task Group 129 by the AAPM and ABS. Med Phys 39:6161-6184. https://doi.org/10.1118/1.4749933
6. Ahmadi P, Gili R (2026) Monte Carlo-based dosimetric comparison of CCA and CCB radioactive eye plaques for uveal melanoma. Phys Eng Sci Med 49:759-769. https://doi.org/10.1007/s13246-026-01701-x
7. Arjmand M, Ghassemi F, Rafiepour P, Zeinali R, Riazi-Esfahani H, Beiki-Ardakani A (2023) Dosimetric investigation of six Ru-106 eye plaques by EBT3 radiochromic films and Monte Carlo simulation. J Biomed Phys Eng 13:309-316. https://doi.org/10.31661/jbpe.v0i0.2010-1206
8. Fardi Z, Taherparvar P (2025) Monte Carlo investigation of dose distribution of two model 106Ru/106Rh ophthalmic plaques in a realistic human eye model with different uveal melanoma size. Appl Radiat Isot 217:111636.
9. Ghassemi F, Sheibani S, Arjmand M, Poorbaygi H, Kouhestani E, Sabour S, Samiei F, Beiki-Ardakani A, Jabarvand M, Sadeghi Tari A (2020) Comparison of iodide-125 and ruthenium-106 brachytherapy in the treatment of choroidal melanomas. Clin Ophthalmol 14:339-346.
10. Jabbarli L, Fiorentzis M, Rating P, Schmidt B, Biewald E, Guberina N, Flühs D, Bornfeld N, Sauerwein W, Stuschke M, Bechrakis NE (2025) Functional outcome after brachytherapy with bi-nuclide (Ru-106/Iodine-125) plaques in large uveal melanomas. Radiat Oncol 20:22.

11. Moeini SM, Sina S, Rafiepour P, Siavashpour Z (2026) Monte Carlo simulation of uveal melanoma treatment by ocular plaque brachytherapy using gold nanoparticles. Radiat Environ Biophys 65:501-518. https://doi.org/10.1007/s00411-026-01206-x
12. Perl J, Shin J, Schumann J, Faddegon B, Paganetti H (2012) TOPAS: an innovative proton Monte Carlo platform for research and clinical applications. Med Phys 39:6818-6837. https://doi.org/10.1118/1.4758060
13. Faddegon B, Ramos-Méndez J, Schuemann J, McNamara A, Shin J, Perl J, Paganetti H (2020) The TOPAS tool for particle simulation, a Monte Carlo simulation tool for physics, biology and clinical research. Phys Med 72:114-121. https://doi.org/10.1016/j.ejmp.2020.03.019
14. Agostinelli S, Allison J, Amako K, Apostolakis J, Araujo H, Arce P et al (2003) Geant4—a simulation toolkit. Nucl Instrum Methods Phys Res A 506:250-303. https://doi.org/10.1016/S0168-9002(03)01368-8
15. Poher A, Berumen F, Ma Y, Perl J, Beaulieu L (2023) Validation of the TOPAS Monte Carlo toolkit for LDR brachytherapy simulations. Phys Med 107:102516. https://doi.org/10.1016/j.ejmp.2022.102516
16. Cullen DE, Hubbell JH, Kissel L (1997) EPDL97: the evaluated photo data library 97 version. Lawrence Livermore National Laboratory, California, USA.
17. Eckert & Ziegler (2021) Fact sheet: Ru-106 eye applicators. Eckert & Ziegler BEBIG GmbH, Berlin. Available at: https://medical.ezag.com/wp-content/uploads/2021/07/Fact-sheet-Ru-106-Eye-Applicators-Rev.08-English_WEB.pdf (Accessed 2 November 2026).
18. L'Annunziata MF (2012) Handbook of radioactivity analysis: table of radioactive isotopes. pp 1305-1360.
19. Rivard MJ, Coursey BM, DeWerd LA, Hanson WF, Saiful Huq M, Ibbott GS et al (2004) Update of AAPM Task Group No. 43 Report: a revised AAPM protocol for brachytherapy dose calculations. Med Phys 31:633-674. https://doi.org/10.1118/1.1646040
20. Atefi S, Rafiepour P, Ahmadi P (2026) Enhancing the therapeutic ratio in prostate LDR brachytherapy: a TOPAS Monte Carlo investigation of nanoparticle radiosensitization. Research Square, Preprint (Version 1), 24 August 2026. https://doi.org/10.21203/rs.3.rs-10499744/v1

Statements and Declarations

Funding

The authors declare that no funds, grants, or other support were received during the preparation of this manuscript.

Competing Interests

The authors have no relevant financial or non-financial interests to disclose.

Author Contributions

All authors contributed to the study conception and design. The main part of simulations and analysis were performed by Shahab Atefi. Final investigations were performed by Payman Rafiepour and Parvin Ahmadi. The first draft of the manuscript was written by Shahab Atefi and all authors commented on previous versions of the manuscript. All authors read and approved the final manuscript.

Ethics approval

Not applicable.

Consent to participate

Not applicable.

Consent to publish

Not applicable.

Availability of data

All data produced from this study will be available from the corresponding author on reasonable request.